

RECCraft System: Towards Reliable and Efficient Collective Robotic Construction

Qiwei Xu, Yizheng Zhang, Shenghao Zhang, Rui Zhao, Zhuoxing Wu, Dongsheng Zhang, Cheng Zhou, Xiong Li, Jiahong Chen, Zengjun Zhao, Luyang Tang, Zhengyou Zhang, Lei Han*

Abstract—This research presents a novel Collective Robotic Construction (CRC) system named RECCraft. The RECCraft hardware system is composed of the mobile manipulation vehicles, the cubic blocks, and the folding ramp blocks. Solid connection and easy removal of the blocks are achieved by an electropermanent magnet and silicon steel sheets. With one degree of freedom (DOF) lifting manipulator, the robot can carry a block 3.7 times its volume. An active folding ramp block can provide a robust passage to the upper level for the robot. Our study focuses on systemic improvement of the construction speed and reliability of the robotic construction system. Visual perception system realized by Apritag is adopted, featured by convenient deployment and high precision, to provide a reliable guarantee for robotic construction. RL-based planner provides end-to-end solution for planning tasks of building multi-layer constructions, which is validated by simulation platform and real prototype. Compared with construction speed of existing robotic construction systems, our proposed RECCraft system achieves state-of-the-art level. The robot builds a 2-layer construction by RL-based planner in 4 minutes and 16 seconds, which achieves construction volumetric throughput of $6.7 \times 10^5 \text{mm}^3/\text{s}$.

I. INTRODUCTION

Collective construction is a common activity in both nature and human society. The worker bees collect raw materials and build a large hive composed of thousands of cells stacked in multiple layers through cooperation. Via teamwork and advanced tools, human beings have been able to build incredibly large buildings compared to human size. Due to the danger of construction and the rising cost of labor force, Collective Robotic Construction (CRC) is believed to be able to improve automation of construction activities. On the other hand, we notice that in the popular virtual game Minecraft, players build various customized virtual constructions using only universal unit blocks as the very fundamental material. This inspires us that the robotic construction platforms can potentially build a bridge from the construction in the virtual world (like Minecraft) to that of the real world.

Based on this motivation, we propose a novel autonomous CRC platform which we refer to as Reliable and Efficient CRC Craft (RECCraft). The target of this project is to build a general hardware and software platform for studies of CRC, with high efficiency and robustness. Key components of the hardware platform include a mobile manipulation builder and two types of heterogeneous building blocks - the cubic block and the folding ramp block. In addition to serving as building materials, the ramp blocks also provide reliable

passages for the builders to reach the upper floor of the construction, which demonstrates cooperation between the builder and building materials. The hardware system focuses on improving construction throughput and manipulation precision of the robotic construction system. As shown in Fig. 1, the builder adopts an 1-DOF lifting mechanism for picking the building blocks, facilitating behaviors of picking and unloading the building blocks. Then, high construction speed of manipulation is realized by sufficient loading capacity of the builder robot, which can pick a block 3.7 times its volume. This is similar to transport behavior of insects in nature. Mechanical characteristics of the block and the manipulator achieve passive positioning alignment of manipulation actions, which increases manipulation precision. Next, we propose to further develop the scalability of the construction system. In this work, we consider construction tasks, while our system is general to accomplish other specified tasks. Specifically, we design a RECCraft simulator via the Bullet engine as a digital copy of the real system. In the simulator, it is easy to design diverse problems covering cooperative, competitive, and co-competitive mixed tasks. Reinforcement learning (RL) algorithms are then applied to train robot's policy in the simulator via an end-to-end scheme, and the policy is then deployed in real robot directly, allowing the robot swarm to build construction much more larger than the robot's size and achieve other complex tasks.

The paper is organized as follows. Section II presents the related work of the CRC system. Section III proposes the concept of the RECCraft system, including three parts: connection/disassembly of blocks, climbing up/down multi-layer blocks as well as picking/placing a block. Section IV presents details of the hardware system. Section V presents the visual localization system. High-level planning is presented in Section VI. In Section VII, construction speed and reliability of the proposed RECCraft system are carefully validated, and demonstrations of building multi-layer constructions are presented. Section VIII concludes the work.

II. RELATED WORK

In CRC literature, researchers have proposed various building elements and builder robots to accomplish construction tasks. Early works of CRC solve the 2D construction of a barrier or a wall [1], [2]. Some recent works develop CRC platforms that are capable of building 2.5D or 3D construction using discrete materials such as bricks, pockets and struts [3]–[5] or continuous building elements such as rope

(*Correspondence to: Lei Han, lxhan@tencent.com)

All of the author are with Tencent Robotics X Lab, Shenzhen, China.



Fig. 1: Overview of the RECCraft platform. The robot is climbing a ramp block and building 3-level construction of blocks. The inner image presents 3 components of the RECCraft hardware system: the mobile manipulation vehicle, the cubic block, and the folding ramp block.

and polyurethane foam [6], [7]. Normally, discrete building materials are picked and placed by a specialized manipulator and the continuous building elements are normally ejected by an extrusion mechanism. These two kinds of building elements have their own advantages and shortages. It is possible to build amorphous construction or fill gaps of the existing structure with continuous material [7]. However, construction removal is much difficult for such building material.

Mobility of reaching upper floor and robust manipulation are important [8] for building multi-layer construction. Both aerial and ground vehicles have been used to serve as transportation tools. Some studies present that the aerial vehicle demonstrates advantage on efficient obstacle-overcoming ability [5], [7]. However, limited payload of the aerial vehicle causes lightweight and comparably small size of building materials. Existing ground vehicles for 2.5D or 3D construction includes wheel-legged vehicle [9], bipedal robot [10] and wheeled robot with assistance of ramp or bridge [11], [12]. Wheel-legged vehicle has good stair-climbing ability, while the stability and success rate of climbing are unsatisfactory. Ramp seems to be a safe and efficient way for climbing [7], [11], [13]. The approach [6] designs a mobile robot that can build a ramp structure by extrusion machine to climb a stair. Another recent work [13] proposes a mobile manipulation robot for unstructured environment, which modifies shape of unstructured terrain.

In addition, environment perception and communication are important concepts that help robots perceive their exact localization. In some previous studies, robots exploit high-resolution sensors and high-speed communication to simulate how animals perceive and communicate with the environment. There are different positioning methods for CRC systems such as global sensors [14], [15] and common templates [1]–[4], [16]. In particular, [17] and [14] both use an overhead motion capture system namely *Vicon* to get the marked object’s position, which is quite convenient but limits the application environment. [3] shows how robots can build a barrier along with heterogeneous template in the environment. The collective structure in [16] provides a reference for robots to keep track of their movements.

Compared with the above approaches, the principle contributions of the proposed RECCraft system include: (1) picking/placing a block realized by 1-DOF manipulation mechanism, resulting in high throughput based on the large block size and facilitation of manipulation; (2) convenient assembly and disassembly of the blocks; (3) foldable ramp block design which provides robust access among different floors of construction for the robot.

III. CONCEPT OF THE SYSTEM

There are three basic units in the RECCraft system, including the mobile manipulation robot, the cubic block, and the active folding ramp block. They cooperate to build multi-layer construction and improve the construction speed and robustness. In our design, the building block is no longer a passive construction unit that it can change its form from a cubic block to a ramp to support the mobile manipulation vehicle accessing to the upper level of construction.

A. Assembly and Disassembly of The Blocks

Electromagnets and silicon steel sheets are respectively arranged on four corners of the lower surface and upper surfaces of the cubic block, as shown in Fig. 2. Connection of the upper and lower blocks is realized by magnetic attraction of the electromagnets and the silicon steel sheets. Magnetization and demagnetization are energized by manipulation of the mobile vehicle. Since the number of the cubic blocks is large, this is a more economical way compared to placing batteries in each block. Most of the time, electromagnets on blocks are magnetic to keep connection between blocks. When the blocks are separated, the electromagnets are powered and changed to demagnetization state. As a result, the electropermanent magnet meets this magnetic properties.

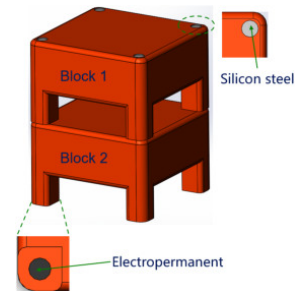


Fig. 2: Concept of assembly of two cubic blocks.

B. Manipulation

As shown in Fig. 3, we design tunnel openings on each vertical side of the block to let the robot pass through. When the mobile manipulation vehicle reaches the bottom center of the cubic block, the lifting mechanism lifts the block and holds it tightly through the attraction of electropermanent magnet. It has the similar lifting behavior to the Kiva robotic platform [18]. The process of picking and placing a block is accurate and efficient thanks to the 1-DOF lifting manipulation. The block is 3.7 times the size of the robot, which highly increases construction throughput.

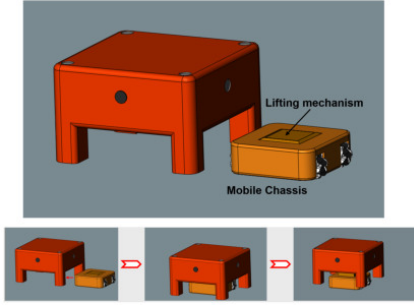


Fig. 3: Concept of picking a block by lifting manipulation.

C. Climbing

Ramp block provides passage to higher level of the construction for the robot. Similarly, the mobile vehicle can lift the folding ramp block and transport it to the target location. Different from the cubic block, the ramp block is powered by inside battery, and it can actively change its status from a folded state (a shape with the same size of a cubic block) to an unfolded state, serving as a ramp with an inclination of about 15° , as shown in Fig. 4. When the mobile vehicle is carrying a ramp block, folded state of the ramp block avoids collision with other existing structure. Then, the center of mass (COM) of the folded ramp block is nearly on the same vertical line as the COM of the mobile vehicle, which improves the stability of transportation.

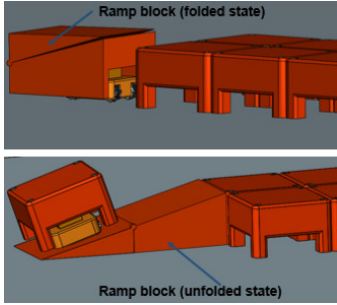


Fig. 4: Concept of climbing to higher level by folding ramp block.

D. Visual localization

Localization system are characterized with the following major points: easy deployment, robustness, and high precision. The local camera on the mobile vehicle is adopted instead of the global sensor, which makes it possible to arrange this robotic platform outdoors. Just We only need to place the aluminum bases with Apritags in some specific order on the ground to let the entire system work. It is simple and efficient to deploy the base ground. Moreover, the smaller Apritags on the block is used for local precise positioning. For structural scenes, such as cubic blocks or ramp blocks, line patrol is deployed to keep the vehicle along the center line. After a long period of testing, the localization system has shown sufficient accuracy to ensure the robustness of the whole system.

IV. HARDWARE

TABLE I: Specifications of the RECCraft hardware platform.

Items	Features
Size of the vehicle	235mm \times 225mm \times 108mm
Size of the cubic block	340mm \times 340mm \times 185mm
Size of the folding ramp block	668 mm \times 340 mm \times 185 mm
Mass of the vehicle	5.2kg
Mass of the cubic block	3.2kg
Mass of the folding ramp block	4.6kg
Rated payload of lifting	53.2N
Max. speed of the vehicle	2m/s (no-load)

A. Mobile Manipulation Vehicle

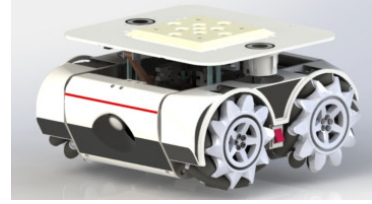


Fig. 5: The mobile manipulation robot with lifting manipulator.

The robot is composed of an omnidirectional mobile chassis and a lifting manipulator, as shown in Fig. 5. Mecanum wheeled chassis is adopted because of its high mobility. The drive system of the mobile chassis consists of four DJI 2006 P36 DC motors, providing a rated angular speed of 416 rpm. Maximum speed of the mobile chassis reaches more than 2 m/s. The lifting manipulator is achieved by symmetric rod-slider mechanism, which converts the rotary motion of DC motor into vertical linear motion of the lifting plate. Torque of DC motors for lifting is transmitted to the left and right swing rod via the gear train, as shown in Fig. 6. Eqs. (1)-(3) presents the relationship between the payload of the lifting plate F_L , the transmission ratio i_{12} and the torque of the DC motor M_1 , respectively. The lifting mechanism is driven by a DJI M3508 motor with rated torque of 3 Nm. Considering transmission efficiency which is about 0.8, the transmission ratio is chosen as 4:3 and the rated payload of lifting is about 53.2 N. As shown in Fig. 7(c), convex with wedge-shaped surface is placed on the lifting plate. The wedge-shaped surface realizes passive positional alignment between the lifting plate and the blocks.

$$F_{L1} = F_{L2} \quad (1)$$

$$F_{L1} \times L \times \cos(\theta) + F_{L2} \times L \times \cos(\theta) - M_1 \times i_{12} = 0 \quad (2)$$

$$F_L = F_{L1} + F_{L2} = \frac{M_1 \times i_{12}}{L \times \cos(\theta)}, \theta \in \left[\frac{\pi}{10}, \frac{\pi}{2} \right] \quad (3)$$

B. Cubic Block

The block is designed as a cube with four surrounding tunnel openings, as shown in Fig. 7. Due to the lifting

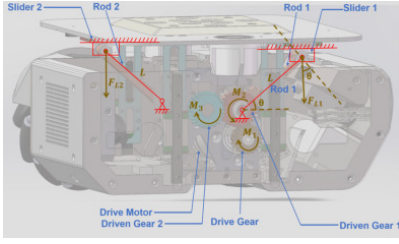


Fig. 6: Lifting mechanism achieved by rod-slider mechanism.

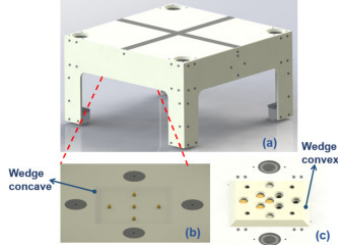


Fig. 7: (a) The Cubic block. (b) Wedge concave on the underside of the block. (c) Wedge convex on the lifting plate.

manipulation design, the volume of the block can reach about 3.7 times the volume of the vehicle. Silicon steel sheets and electropermanent magnets are respectively placed on the four corners of the upper surface and the lower surface. Each electropermanent magnet provides about 100N of normal magnetic force and 25N of tangential magnetic force. When the lifting plate touches the bottom of the block, power supply connectors on the lifting plate are in contact with the positive and the negative copper sheets placed at the bottom of the block. Degaussing of the electropermanent magnet can be directly controlled by on-off control command from the mobile manipulation vehicle. Since the error of visual localization and control is inevitable, some fault-tolerant mechanical features are adopted. As presented in Fig. 7(b), a wedged concave is designed on the underside of the block. When the manipulation mechanism lifts the block, passive alignment of wedged concave on the block and wedged convex on the lifting plate provides positional error tolerance of 10 mm to compensate stochastic error of motion control.

C. Folding Ramp Block

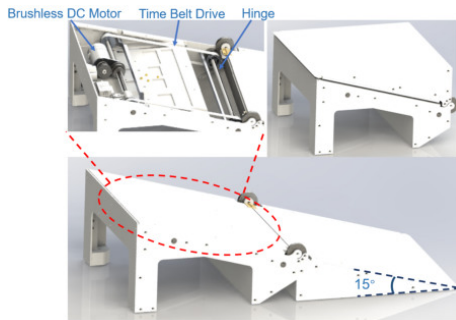


Fig. 8: Lifting mechanism achieved by rod-slider mechanism.

Switch of the folded and unfolded states of the ramp block

is achieved by an actively actuated hinge mechanism, as shown in Fig. 8. Unfolded state of the ramp block is a ramp with an inclination of 15° . When the lifting plate picks the folded ramp block, the overall COM should be as close as possible to the central axis of the lifting plate to increase stability of motion. Then, actuation of the hinge is placed on the other side of the block, and torque is transmitted to the hinge via belt transmission, as shown in Fig. 8(b). The design of the passive alignment and magnetic absorption of the lifting surface is the same as that of the cubic block. The actuation of the hinge is driven by a DJI M3508 motor. The surface of the ramp is covered with a layer of anti-slip tape. After the mobile manipulation vehicle places the folded ramp block to the target localization, it sends control commands to the ramp via wireless signal, and the ramp block unfolds.

D. Electronics

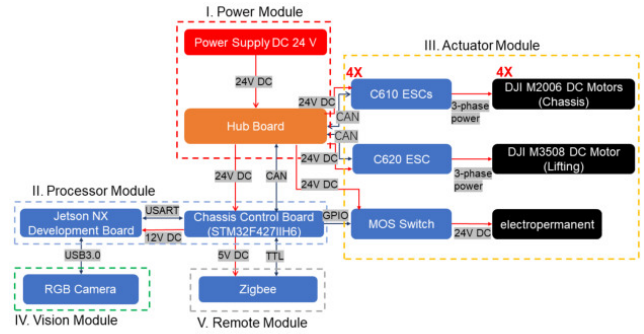


Fig. 9: Electronics framework of the mobile manipulation vehicle.

As shown in Fig. 9, the electronics of the mobile manipulation vehicle includes five modules: the power supply module, the processor module, the actuator module, the vision module and the remote module. The hub board is the hub for power and CAN communication. A 24V Lithium battery powers the hub board, and the hub board powers the actuator module and the chassis control board. The hub board also bridges CAN communication among the chassis control board and the ESCs. A MOS switch accepts the GPIO signal from the chassis control board, which is used to change the on-off of the electropermanent magnets on the lifting plate. The Jetson NX development board serves as an upper computer dealing with visual localization computing and sends action commands to the chassis's control board via USART. An RGB camera generates images at 50Hz for visual localization. A Zigbee module is used for wireless communication between the vehicle and the folding ramp block.

V. VISUAL LOCALIZATION

A. Hardware Setup and Calibration

The visual perception system is designed simply based on one camera, which is a 960×600 monochrome camera equipped with a 180-degree wide-angle lens.

TABLE II: An example of visual localization.

Case number	1	2	3	4	5	6	7	8	9	10	11	12	13
Current state	(x_c, y_c)												
Starting area number N_s	1	2	3	3	4	5	5	6	7	7	8	1	
Ending area number N_e	7	6	5	1	8	7	3	2	1	5	4	3	Others
Flag(= $N_s * 10 + N_e$)	17	26	35	31	48	57	53	62	71	75	84	13	
Next state	$(x_c, y_c + 1)$			$(x_c + 1, y_c)$			$(x_c, y_c - 1)$			$(x_c - 1, y_c)$			(x_c, y_c)

To unify the vision and control coordinate system, calibration of the transformation relationship T_{camera}^{car} from the camera to the COM of the vehicle is conducted, with the help of a grid of AprilTag [19] markers with known dimensions. As each AprilTag marker has a unique identifier, it is easy for us to get the camera pose T_{vision}^{camera} . It is evident that $T_{camera}^{car} = T_{vision}^{camera}^{-1} * T_{vision}^{car}$.

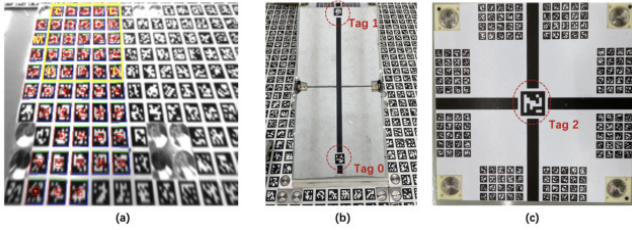


Fig. 10: AprilTag Layout. (a) Ground; (b) Ramp; (c) Block.

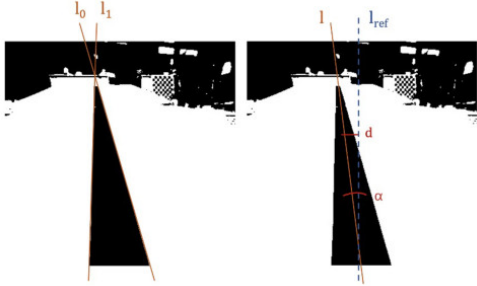


Fig. 11: Line patrol process. The boundaries l_0 and l_1 of the black line are detected and their median line l . l_{ref} denotes the center line of the image.

B. AprilTag Layout

We adopt AprilTag markers for location of the mobile vehicle, as detailed in the following:

- **Ground.** The ground is covered with AprilTag markers to ensure continuous positioning. Unlike previous methods, multiple tags are deployed in the field of view to make the positioning result more robust. As shown in Fig. 10(a), for the detected tags, we can identify the largest square (denoted as M) they can form. The location of the vehicle is determined by the four vertices of M .
- **Folding ramp block.** As shown in Fig. 10(b), the bottom and top of the ramp are marked with unique tags (Tag 0 and Tag 1). When going uphill, Tag 0 and

Tag 1 correspond to the starting state and ending state respectively, with the opposite for going downhill.

- **Cubic block.** As shown in Fig. 10(c), another unique tag is set (Tag 2) at the center of the block, which is used to mark how many blocks the vehicle has passed through. Moreover, we also set some small tags around the block to help us with local positioning on the block.
- **Line patrol.** When the vehicle travels on the ramp and the block, positioning is discrete and line patrol is deployed to keep the vehicle along the center line without falling off. First, we globally binarize the original image. As shown in Fig. 11, we detect lines with the help of Hough transform [20]. Finally, the median line l of l_0 and l_1 are computed, and the angle α and distance d offset of line l relative to the center line l_{ref} of image are obtained.

C. Visual Localization

To cover a large area of ground (made of aluminum bases) with limited kinds of AprilTag markers, we design a method for AprilTag marker reuse. The reused template B contains 32×32 different AprilTag markers. If the area is large enough, we can use an unlimited number of B to cover the ground, only requiring to align their boundaries. As Fig. 12 shows, B is divided into 9 areas, and each area is assigned a corresponding number. When the mobile vehicle is traveling on the areas, assuming that it is currently located at the template numbered (x_c, y_c) , there are 13 cases as shown in Table II. The following equation shows our method to locate the vehicle in the whole map:

$$\begin{cases} x = x_b + x_c * l_b, \\ y = y_b + y_c * l_b, \\ z = z_b, \end{cases} \quad (4)$$

in which (x_b, y_b, z_b) represents the position of the template, (x, y, z) denotes the vehicle position in the whole map, and l_b denotes the template size.

When there are tags from different areas in the field of view, tags from the area which include the largest number of tags for localization are selected.

VI. HIGH-LEVEL PLANNING

We focus on the reliability and generality of the RECCraft system. One way to validate this is to apply high-level control policies upon the RECCraft system to test its performance. In recent years, reinforcement learning (RL) has been demonstrated effective in solving online decision problems. Great achievements have been witnessed in applications of game AI [21], [22], robotics manipulation [23], resource

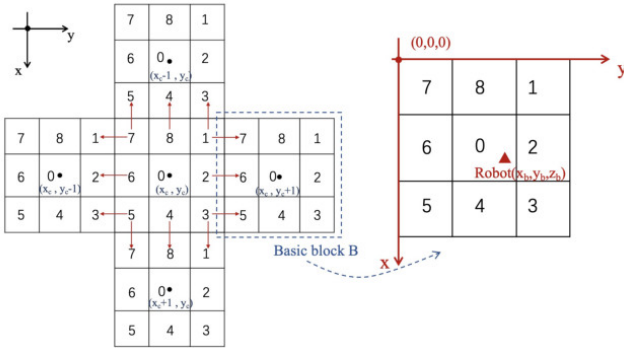


Fig. 12: When the mobile vehicle crosses the templates, there are 12 cases as indicated by the red arrow.

management [24], etc. In this section, we also apply deep RL method to learn the control policy for the vehicle. RL requires frequently interacting with an environment to obtain a large number of trajectories. It is not practical to directly let the RL agent interact with the RECCraft system in reality. Therefore, we build a simulation environment that mimics the real system, using the Bullet engine. A screenshot of the simulation environment is provided in Fig. 13. The vehicle, cubic block and ramp block in the simulation environment strictly follow the physical attributes of the real objects in the RECCraft system.

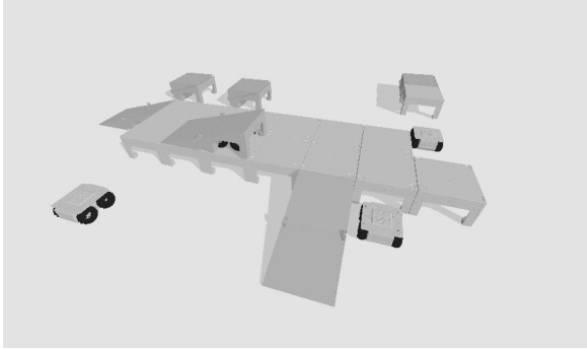


Fig. 13: The simulation environment.

In the RECCraft simulation environment, the agent (i.e., the mobile vehicle) observes a 3D grid space and chooses its action from a set of 10 actions, including moving forward/back/left/right, turning left/right, lifting cubic/ramp block, dropping cubic/ramp block, folding/unfolding ramp block. The agent is assigned a target construction pattern, which should be built by the agent by collecting randomly scattered blocks (which can speedup the RL training process with more random diversity). A standard RL problem can be described by a tuple $\langle E, A, S, P, r, \gamma, \pi \rangle$, where E indicates the environment that is an MDP with dynamics transition probability P ; at each time step t , $s_t \in S$ is the global state in the state space S , and $a_t \in A$ is the action executed by the agent at time step t from the action space A ; the dynamics transition function $P(s_{t+1}|s_t, a_t)$ is the probability of the state transition $(s_t, a_t) \rightarrow s_{t+1}$; for the most general case, the reward $r(s_t, a_t, s_{t+1})$ can be written as a function

of s_t, a_t and s_{t+1} , while in many tasks it only relies on one or two of them, or it is even a constant in sparse rewards problem. For notation simplicity, we usually write $r(s_t, a_t, s_{t+1})$ as r_t ; $\gamma \in [0, 1]$ is a discount factor and $\pi(a_t|s_t)$ denotes a stochastic policy. The following equations define some important quantities in reinforcement learning.

$$J(\pi) = E_{s_0, a_0, \dots \sim P, \pi} \left[\sum_{t=0}^{\infty} \gamma^t r_t \right], \text{ where } s_0 \sim P(s_0),$$

$$a_t \sim \pi(a_t|s_t), s_{t+1} \sim P(s_{t+1}|s_t, a_t).$$

At time step t , the state-action value Q^π , value function V^π , and advantage A^π are defined as $Q^\pi(s_t, a_t) = E_{s_{t+1}, a_{t+1}, \dots \sim P, \pi} [\sum_{l=0}^{\infty} \gamma^l r_{t+l}]$, $V^\pi(s_t) = E_{a_t, s_{t+1}, \dots \sim \pi} [\sum_{l=0}^{\infty} \gamma^l r_{t+l}]$, and $A^\pi(s, a) = Q^\pi(s, a) - V^\pi(s)$. A widely applied RL algorithm is PPO [25], which solves the following optimization problem

$$E_{s \sim d^{\pi_{\theta_{old}}}, a \sim \pi_{\theta_{old}}} \left[\min (R(\theta) A^{\pi_{\theta_{old}}}(s, a), \text{clip}(R(\theta), 1 - \epsilon, 1 + \epsilon) A^{\pi_{\theta_{old}}}(s, a)) \right],$$

where $R(\theta) = \frac{\pi_\theta(a|s)}{\pi_{\theta_{old}}(a|s)}$ and ϵ is a hyperparameter controlling the proportion of clipped data. In our implementation, we adopt PPO as the baseline RL algorithm. The performance of the convergent agent is provided in a demo video in the supplementary material. This verifies that our CRC system is easily applied with high-level control methods, such as general RL.

In multi-agent settings, the robots learn to coordinate with each other through reinforcement learning. A centralized reward function is defined to encourage all the agent in the team to achieve a common goal. The agents need to cooperate with each other to achieve the goal. For example, to build a complex construction efficiently, different agents should work on different parts of the construction simultaneously. The RL-based assembly planner can scale through a Centralized Training and Decentralized Execution (CTDE) framework [26], [27], where during training, we have a centralized value function that processes the information collected by all the robots and calculates the credits and assigns these credits to each robot in the team. During execution, each robot only needs to know its own partial observation, which reduces load of computing for each robot.

VII. EXPERIMENT AND DEMONSTRATION

In this section, validation of the robustness and construction speed of the RECCraft system are conducted by simple tasks and multi-layer construction. Aluminum bases are prepared for experimental purpose, which are covered with grids of the same length and width as the block. Silicon steel sheets are installed on the four corners of the grids.

A. Robustness of Mobile Manipulation

Motion control among grids is realized by combination of OBVP motion planner and PID controller. The PID control includes a coarse position PID controller and a fine-tuning position PID controller.

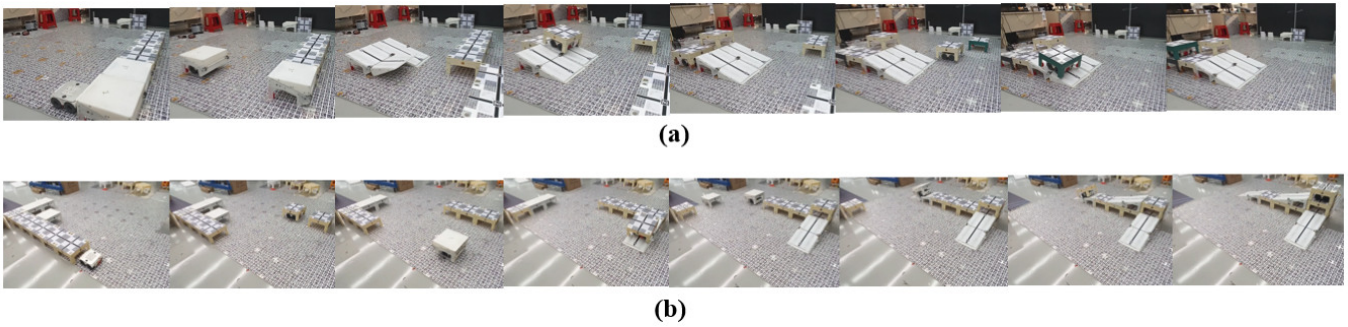


Fig. 15: Demonstration of autonomously building multi-layer construction: (a) Building 2-layer construction by RL-based planning in 4 minutes 16 seconds. (b) Building 3-layer construction by preplanned actions in 6 minutes 25 seconds.

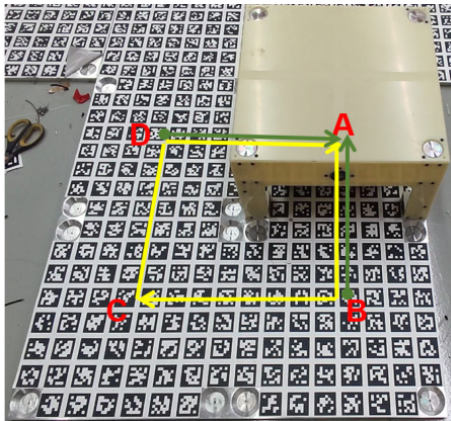


Fig. 14: Experiments of picking/placing a block on the ground. Yellow route: route of placing a block. Green route: route of picking a block.

TABLE III: Success rate and time expanse of placing a block.

	Time of fine tuning (s)	Time of placing (s)	Total (s)	Success rate
Average	4.34	1.51	5.85	100%
Max.	5.02	1.55	6.57	
Min.	3.87	1.46	5.33	

As shown in Fig. 14, points A, B, C and D are the center points of the four adjacent grids on the testbed, respectively. In 1000 trials of placing a block, the robot moves circularly between points A, B, C and D, and sequentially picks/places the block at point A and point C. A successful trial of picking and placing a block indicates that electropermanent magnets and silicon steels are attached without positional deviation. As shown in Table III and Table IV, the system achieves 100% success rate in 1000 trials of picking and placing. The average total time expanse of placing a block is 5.85s and that of picking a block is 5.13s.

B. Building Multi-Layer Construction

In building tasks realized by high level planner, sequences of robot actions consist of picking/placing a block, moving ahead/back/left/right, climbing up/down, folding/unfolding a ramp block. The robot builds multi-layer construction by a well-trained RL-based planner or pre-planned actions. As

TABLE IV: Success rate and time expanse of picking a block.

	Time of fine Tuning (s)	Time of lifting (s)	Total (s)	Success rate
Average	3.14	1.99	5.13	100%
Max.	4.21	2.51	6.71	
Min.	2.58	1.42	4.00	

shown in Fig. 15(a), the robot builds a 2-layer construction with 6 cubic blocks and 2 ramp blocks by RL-based planner in 4 minutes 16 seconds, which achieves construction throughput of $6.7 \times 10^5 \text{ mm}^3/\text{s}$. As shown in Fig. 15, the robot builds a 3-level construction with 6 cubic blocks and 3 ramp blocks by pre-planned action sequence in 6 minutes 25 seconds, which achieves construction throughput of $5.0 \times 10^5 \text{ mm}^3/\text{s}$. Demonstration video of building multi-layer construction is attached to the video document.

VIII. CONCLUSIONS

In this paper, we present an autonomous robotic construction platform with high construction speed. With the assistance of the folding ramp block, the mobile manipulation robot robustly climbs to the upper layer of construction. Then, 1-DOF lifting mechanism as well as passive mechanical alignment of the lifting plate and the blocks realize efficient (about 5s - 6s for picking or placing a block) and robust manipulation (success rate of 100% for picking and placing a block). With energization and degaussing of the electropermanent magnet powered by the lifting plate, a block is easily removed from the construction. The position error of visual localization achieved by Apriltags is within 10 mm on the ground and 2 mm on the block, which provides a reliable localization for lifting and placement of blocks. The robotic system finishes building task by RL-based planner of 2-level construction with 8 blocks in 4 minutes 16 seconds and building tasks by pre-planned action sequence of 3-level construction with 9 blocks in 6 minutes 25 seconds. For comparison of construction speed of the construction system, [8] proposes the metric ‘‘Structure volume per robot-unit-minute’’ and [28] proposes the volumetric throughput. Using these metrics, we compare the construction efficiency of our system with other existing discrete construction systems in Table V. From the results, our construction system demon-

TABLE V: Comparison of construction speed of typical prototypes of discrete construction.

	RECCraft (Ours)	Termes [9]	Material-Robot [28]	Cubic-UAV [29]	Bricks-UAV [17]	2D-Bricks [30]
Mobility	Ground	Ground	Ground	Flying	Flying	Stationary
Throughput (mm^3/s)	6.7×10^5	1.5×10^4	2.0×10^4	1.0×10^5	1.0×10^5	1.33
Volume per robot-unit-minute [8]	7.0	0.87	1.41	3.93	0.34	–

strates advanced throughput of $6.7 \times 10^5 mm^3/s$ and structure volume per robot-unit-time of 7.0. Both metrics indicate that construction speed of the RECCraft system reaches a new state-of-the-art level.

For future work, the RECCraft system could serve as a generalized platform for swarm intelligence research. It is also possible to help creating industrial robotic system which builds multi-layer storage racks for unmanned warehouses, like Kiva robotic system [18]. We are also interested in benchmarking different methods with the RECCraft system, including deterministic and provable algorithms and other RL methods, to compare their performance.

REFERENCES

- [1] Robert L Stewart and R Andrew Russell. A distributed feedback mechanism to regulate wall construction by a robotic swarm. *Adaptive Behavior*, 14(1):21–51, 2006.
- [2] Jens Wawerla, Gaurav S Sukhatme, and Maja J Mataric. Collective construction with multiple robots. In *IEEE/RSJ international conference on intelligent robots and systems*, volume 3, pages 2696–2701. IEEE, 2002.
- [3] Michael Allwright, Navneet Bhalla, Haitham El-faham, Anthony Antoun, Carlo Pinciroli, and Marco Dorigo. Srocs: Leveraging stigmergy on a multi-robot construction platform for unknown environments. In *International conference on swarm intelligence*, pages 158–169. Springer, 2014.
- [4] Touraj Soleymani, Vito Trianni, Michael Bonani, Francesco Mondada, and Marco Dorigo. Bio-inspired construction with mobile robots and compliant pockets. *Robotics and Autonomous Systems*, 74:340–350, 2015.
- [5] Quentin Lindsey, Daniel Mellinger, and Vijay Kumar. Construction of cubic structures with quadrotor teams. *Proc. Robotics: Science & Systems VII*, 7, 2011.
- [6] Nils Napp and Radhika Nagpal. Distributed amorphous ramp construction in unstructured environments. *Robotica*, 32(2):279–290, 2014.
- [7] Federico Augugliaro, Ammar Mirjan, Fabio Gramazio, Matthias Kohler, and Raffaello D’Andrea. Building tensile structures with flying machines. In *2013 IEEE/RSJ International Conference on Intelligent Robots and Systems*, pages 3487–3492. IEEE, 2013.
- [8] Kirstin H Petersen, Nils Napp, Robert Stuart-Smith, Daniela Rus, and Mirko Kovac. A review of collective robotic construction. *Science Robotics*, 4(28):eaau8479, 2019.
- [9] Kirstin Hagelskjaer Petersen, Radhika Nagpal, and Justin K Werfel. Termes: An autonomous robotic system for three-dimensional collective construction. *Robotics: science and systems VII*, 2011.
- [10] Ben Jenett and Kenneth Cheung. Bill-e: Robotic platform for locomotion and manipulation of lightweight space structures. In *25th AIAA/AHS Adaptive Structures Conference*, page 1876, 2017.
- [11] Tarik Tosun, Jonathan Daudelin, Gangyuan Jing, Hadas Kress-Gazit, Mark Campbell, and Mark Yim. Perception-informed autonomous environment augmentation with modular robots. In *2018 IEEE International Conference on Robotics and Automation (ICRA)*, pages 6818–6824. IEEE, 2018.
- [12] Yiwen Hua, Yawen Deng, and Kirstin Petersen. Robots building bridges, not walls. In *2018 IEEE 3rd International Workshops on Foundations and Applications of Self* Systems (FAS* W)*, pages 154–159. IEEE, 2018.
- [13] Vivek Thangavelu, Maíra Saboia da Silva, Jiwon Choi, and Nils Napp. Autonomous modification of unstructured environments with found material. In *2020 IEEE International Conference on Robotics and Automation (ICRA)*, pages 7798–7804. IEEE, 2020.
- [14] Seung-kook Yun, Mac Schwager, and Daniela Rus. Coordinating construction of truss structures using distributed equal-mass partitioning. In *Robotics Research*, pages 607–623. Springer, 2011.
- [15] Alexander Grushin and James A Reggia. Stigmergic self-assembly of prespecified artificial structures in a constrained and continuous environment. *Integrated Computer-Aided Engineering*, 13(4):289–312, 2006.
- [16] Justin Werfel, Kirstin Petersen, and Radhika Nagpal. Designing collective behavior in a termite-inspired robot construction team. *Science*, 343(6172):754–758, 2014.
- [17] Federico Augugliaro, Sergei Lupashin, Michael Hamer, Cason Male, Markus Hehn, Mark W Mueller, Jan Sebastian Willmann, Fabio Gramazio, Matthias Kohler, and Raffaello D’Andrea. The flight assembled architecture installation: Cooperative construction with flying machines. *IEEE Control Systems Magazine*, 34(4):46–64, 2014.
- [18] Raffaello D’andrea, Peter K Mansfield, Michael C Mountz, Dennis Polic, and Patrick R Dingle. Method and system for transporting inventory items, November 2 2010. US Patent 7,826,919.
- [19] Edwin Olson. Apriltag: A robust and flexible visual fiducial system. In *2011 IEEE international conference on robotics and automation*, pages 3400–3407. IEEE, 2011.
- [20] Dana H Ballard. Generalizing the hough transform to detect arbitrary shapes. *Pattern recognition*, 13(2):111–122, 1981.
- [21] Volodymyr Mnih, Koray Kavukcuoglu, David Silver, Andrei A Rusu, Joel Veness, Marc G Bellemare, Alex Graves, Martin Riedmiller, Andreas K Fidjeland, and Georg Ostrovski. Human-level control through deep reinforcement learning. *Nature*, 518(7540):529, 2015.
- [22] David Silver, Julian Schrittwieser, Karen Simonyan, Ioannis Antonoglou, Aja Huang, Arthur Guez, Thomas Hubert, Lucas Baker, Matthew Lai, and Adrian Bolton. Mastering the game of go without human knowledge. *Nature*, 550(7676):354, 2017.
- [23] Jens Kober, J Andrew Bagnell, and Jan Peters. Reinforcement learning in robotics: A survey. *The International Journal of Robotics Research*, 32(11):1238–1274, 2013.
- [24] Hongzi Mao, Mohammad Alizadeh, Ishai Menache, and Srikanth Kandula. Resource management with deep reinforcement learning. In *Proceedings of the 15th ACM Workshop on Hot Topics in Networks*, pages 50–56, 2016.
- [25] John Schulman, Filip Wolski, Prafulla Dhariwal, Alec Radford, and Oleg Klimov. Proximal policy optimization algorithms. *arXiv preprint arXiv:1707.06347*, 2017.
- [26] Jakob Foerster, Gregory Farquhar, Triantafyllos Afouras, Nantas Nardelli, and Shimon Whiteson. Counterfactual multi-agent policy gradients. In *Proceedings of the AAAI Conference on Artificial Intelligence*, volume 32, 2018.
- [27] Ryan Lowe, Yi Wu, Aviv Tamar, Jean Harb, Pieter Abbeel, and Igor Mordatch. Multi-agent actor-critic for mixed cooperative-competitive environments. In *Advances in Neural Information Processing Systems*, pages 6379–6390, 2017.
- [28] Benjamin Jenett, Amira Abdel-Rahman, Kenneth Cheung, and Neil Gershenfeld. Material-robot system for assembly of discrete cellular structures. *IEEE Robotics and Automation Letters*, 4(4):4019–4026, 2019.
- [29] Quentin Lindsey, Daniel Mellinger, and Vijay Kumar. Construction with quadrotor teams. *Autonomous Robots*, 33(3):323–336, 2012.
- [30] Will Langford, Amanda Ghassaei, and Neil Gershenfeld. Automated assembly of electronic digital materials. In *International Manufacturing Science and Engineering Conference*, volume 49903, page V002T01A013. American Society of Mechanical Engineers, 2016.